Supplementary Material

Perfluorocarbon nanodroplets can reoxygenate hypoxic tumors *in vivo* without carbogen breathing

Yun Xiang,[1*] Nicholas Bernards,[2*] Bryan Hoang,[1,2] Jinzi Zheng[2,3] and Naomi Matsuura[1,3,4]

[1]Department of Medical Imaging, University of Toronto, Ontario, Canada

[2]TECHNA Institute for the Advancement of Technology for Health, University Health Network, Toronto, Ontario, Canada

[3]Institute of Biomaterials and Biomedical Engineering, University of Toronto, Ontario, Canada

[4]Department of Materials Science and Engineering, University of Toronto, Ontario, Canada

[*]These authors contributed equally to this work.

1. Fluorescence intensity

The fluorescence emission spectrum of DiI-labeled PFOB nanodroplets at various dilutions was measured by fluoremetry (Figure S1). Using an excitation wavelength of 549 nm, the emission peak was 565 nm. Since this emission peak is very close to the excitation wavelength and would impact the organ-based fluorescence analysis using the Maestro hyperspectral fluorescence system, instead of measuring fluorescence at 565 nm, the secondary peak at 610 nm was used for quantitative measurement (Figure S1).

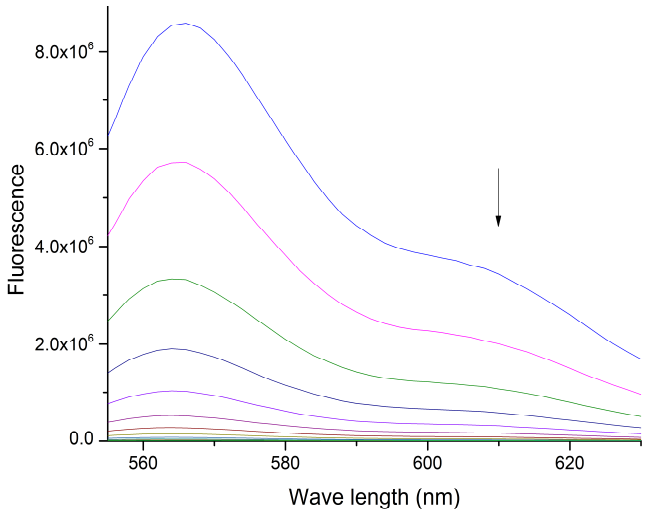

Figure S1. The fluorescence emission spectra of the DiI labeled PFOB nanoemulsion dilutions. The primary emission peak was 565 nm and the secondary emission peak was 610 nm (arrow).

2. [^{18}F]FAZA PET imaging

To evaluate the reoxygenation effect derived from PFOB nanodroplets accumulated in tumors, [^{18}F]FAZA PET imaging was used. Approximately 30 days post-inoculation with tumor cells, the PFOB nanodroplets were administrated into mice 24 hours before the [^{18}F]FAZA injection, while carbogen breathing was initiated 2 hours before the [^{18}F]FAZA injection. The PET images was obtained 2 hours after the [^{18}F]FAZA injection (Figure S2).

The coronal, sagittal, and axial segmented images of the tumor from a representative animal of each group is shown in Figure S3.

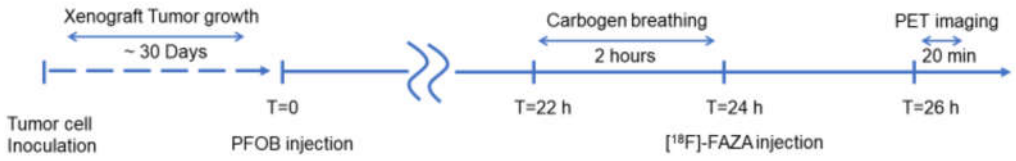

Figure S2. Schematic timeline of the *in vivo* experiment, using PET imaging with [^{18}F]FAZA to evaluate the reoxygenation effect of PFOB nanodroplets.

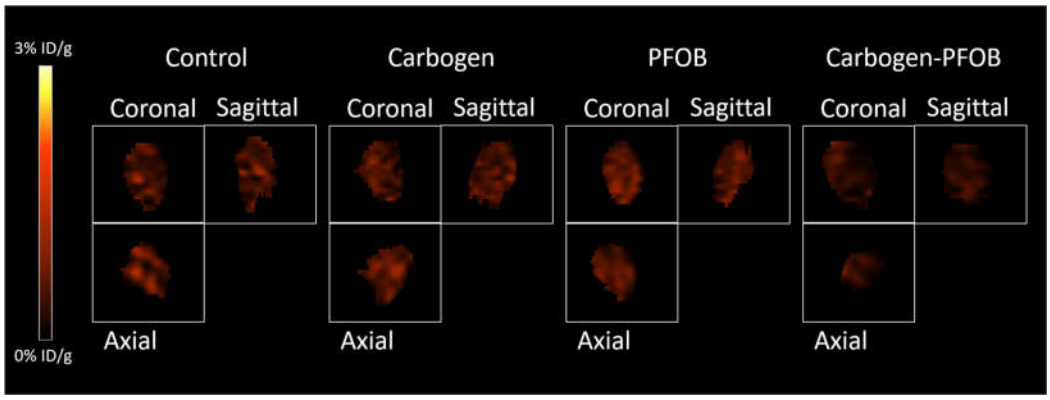

Figure S3. The coronal, sagittal, and axial segmented images of a central tumor slice from a representative animal from each group.

3. Simulation

The simulation of oxygen diffusion from the blood vessel into the tissue bed was carried out on the COMSOL Multiphysics 2-D model representing the cross-section of both the blood vessel and its surrounding tissue. The simulation was based on the Fick's laws of diffusion. By balancing the oxygen consumption in the tissue and the oxygen supply from the vessel, the model determines the distance that oxygen can diffuse before its concentration falls below the threshold of hypoxia. To counteract the hypoxia derived from the abnormal large intercapillary distance (ICD) in the tumor, reoxygenation typically increases the diffusion distance of oxygen from the blood vessel before it falls below the threshold. Several assumptions were made in this simulation. First, the tissue oxygen solubility and diffusivity were assumed to be uniform in the tissue. Second, the axial oxygen diffusion in both tissue and blood vessel was assumed to be negligible (i.e., only the diffusion and consumption of oxygen in the radial direction were considered). Third, only one blood vessel was simulated after reaching equilibrium.

A summary of tissue parameters used in the analysis is shown in Supplementary Table S1. Diffusion efficiency (i.e., the diffusivity of oxygen) in tissue, D_T, is highly dependent on the types of tissue. A value close to that in water ($D_T=2\times10^{-9}$ m^2/s) was used in this study [1–4]. Henry's constant in both plasma and tissue (H and H_T) were set as 0.75 mmHg/μM [5]. The radius of the capillary in tumor tissue varies between 5 to 10 μm, so here was set at 7 μm [3,6,7].

In the simulation, the oxygen consumption rate is calculated to obey a rectangular hyperbolic relationship, similar in form to M-M kinetics. This model has been shown to be a good approximation of various tissues, including tumor tissue. The consumption rate is obtained by:

$$\Gamma = \frac{\Gamma_{max} \cdot P_T}{P_T + K_m}$$

where P_T is the oxygen partial tension of tissue, Γ_{max} is the maximum consumption rate and K_m is the P_T level where Γ is half Γ_{max}. Literature indicates that the constant K_m is quite low for oxygen compared with typical oxygen partial tension. Here, Γ is set as a constant of 15 mmHg/s, corresponding to 20 μM/s [8,9].

Table S1. Numerical values for the physical parameters in the Krogh model.

Parameter	Value	Unit	
Capillary radius (r_0)	7	μm	[3,6,7]
Diffusivity of oxygen in tissue (D_T)	2×10^{-9}	m^2/s	[1–4]
Diffusivity of oxygen in PFC (D_{PFC})	5.6×10^{-9}	m^2/s	[6,10]
Henry's constant of oxygen in tissue (H_T)	0.75	mmHg/μM	[5]
Henry's constant of oxygen in PPFC (H_{PFC})	0.04	mmHg/μM	[5,11]
Oxygen consumption rate of tissue (Γ)	20	μM/s	[8,9]

In normoxic tissue, the inlet oxygen partial tension is set at 75 mmHg [12]. The normoxic region was shown as the area inside the red circle (Figure S1a). During carbogen breathing, the oxygen partial tension in the lung increases 4 to 5 times, but the oxygen partial tension in blood vessels significantly drops from arteries to the arterioles and capillaries before it reaches the tumor [13,14]. Thus, in this simulation, a two-fold increase of oxygen partial tension was applied. Based on the simulation, the increased oxygen partial tension from the blood vessel significantly enlarge the normoxic region (the area inside the yellow circle) compared with the control (Figure S2b).

In the PFC nanodroplet case, the PFC nanodroplets accumulated in tumor tissue serve to dynamically balance their oxygen partial tension with the surrounding tissue because of its high oxygen solubility and diffusivity, while continually diffusing oxygen into the surrounding solid tumor. The intratumoral distribution of nanoscale agents is difficult to predict. It is governed by parameters such as agent size, surface charge, and its interaction with the tumoral extracellular matrix (ECM) where the collagen density in solid tumor tissue is negatively correlated to the diffusion of most nanoscale agent [15,16]. In the case of PFC emulsions aggregated around the blood vessel, the clustered nanodroplets balance its oxygen partial tension with the blood vessel immediately due to its high oxygen solubility and diffusivity and shortens the diffusion distance. However, aggregated PFC nanodroplets do not efficiently enlarge the normoxic region.

For example, a 20 micron-size aggregate of PFC nanodroplets only expands the normoxic region 32 microns in that direction (Figure S1c).

In the case of PFC emulsions evenly distributed in the tumor tissue, the presence of PFC nanodroplets increased the tumor's oxygen permeability. According to the parallel model, the apparent oxygen solubility of the mixture follows:

$$a_{app} = \varphi \cdot a_{PFC} + (1 - \varphi) \cdot a$$

where *a, $a_{PFC,}$ and a_{app}* represent the oxygen solubility in tissue, the oxygen solubility in PFC, and the apparent solubility of the mixture, respectively [17]. Typically, the solubility is the reciprocal of Henry's constant. In this equation, φ represents the volume ratio of PFC.

In addition, the apparent diffusivity (D_{app}) of the mixture can also be determined by:

$$D_{app} = \varphi \cdot D_{PFC} + (1 - \varphi) \cdot D$$

where D_{PFC} represent the oxygen diffusivity in PFC (5.6×10^{-9} m^2/s) [6,10].

The simulation shows that the evenly distributed PFC nanodroplets expand the normoxic region in all direction. The size of the enlarged normoxic region became comparable to carbogen breathing when the amount of PFC reached 8% v/v of the whole tumor (Figure S1d). In reality, the distribution PFC nanodroplets in the tumor will likely be neither fully aggregated around vessels nor totally evenly distributed throughout the tumor. Furthermore, the percentage of the total injected dose that is expected to reach the tumor in preclinical models is below 10% even the EPR targeting is applied [18], suggesting that this model requires substantially more nanodroplet accumulation than is realistically feasible to match the expected oxygenation effect due to carbogen breathing.

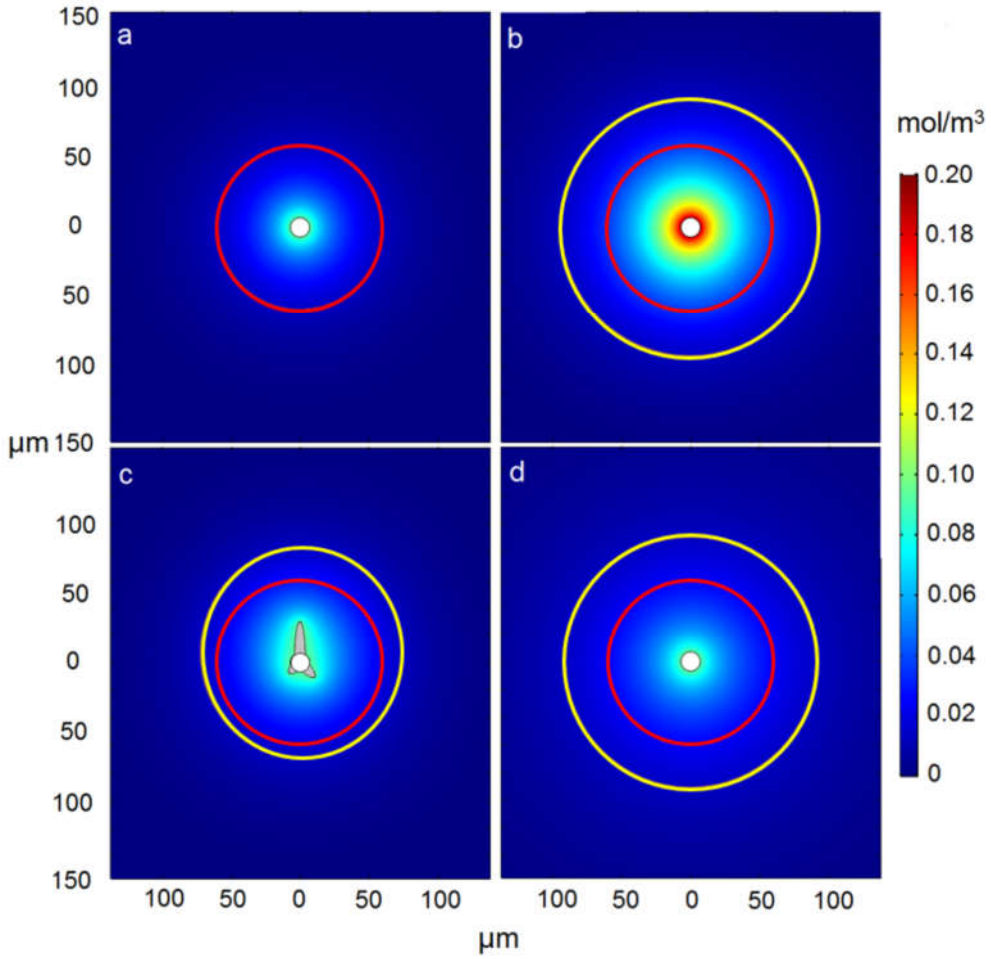

Figure S4. Simulations of oxygen diffusion from blood vessels (white circles in the center of each frame) into the surrounding tissue. The oxygen concentration (in mol/m^3) surrounding the blood vessel is shown using a color scale. (a) Simulation of normoxia with 75 mmHg oxygen partial tension from the blood vessel. The tissue outside the red circle represents oxygen partial tension below 10 mmHg and thus represents the hypoxic region, while the tissue inside the circle represents the normoxic region. (b) Carbogen breathing raises the oxygen partial tension up to 150 mmHg and expands the normoxic region (yellow circle). (c) PFC nanodroplets accumulated as cluster surround the blood vessel is shown in grey. The asymmetric aggregation of the PFC nanodroplets leads to an asymmetric region of normoxia (as outlined in yellow circle). (d) PFC nanodroplets evenly distributed in the tissue surrounding the blood vessel (here, representing 8% v/v of the total tumor volume) leads to an increased normoxic region (as in yellow circle).

References

1. Grote J, Susskind R, Vaupel P. Oxygen Diffusivity in Tumor Tissue (DS-Carcinosarcoma) under Temperature Conditions within the Range of 20-40. Pflugers Archiv European Journal of Physiology. 1977; 2: 3–8.
2. MacDougall JD, McCabe M. Diffusion coefficient of oxygen through tissues. Nature. 1967; 215: 1173–1174.
3. Schumacker PT, Samsel RW. Analysis of oxygen delivery and uptake relationships in the Krogh tissue model. Journal of applied physiology (Bethesda, Md : 1985). 1989; 67: 1234–1244.
4. Pogue BW, Hara JAO, Wilmot CM, et al. Estimation of Oxygen Distribution in RIF-1 Tumors by Diffusion Model-Based Interpretation of Pimonidazole Hypoxia and Eppendorf Measurements. Radiation research. 2001; 155: 15–25.
5. Fournier R. Basic Transport Phenomena in Biomedical Engineering. 2000; .
6. Radisic M, Deen W, Langer R, et al. Mathematical model of oxygen distribution in engineered cardiac tissue with parallel channel array perfused with culture medium containing oxygen carriers. American journal of physiology Heart and circulatory physiology. 2005; 288: H1278-1289.
7. Skeldon AC, Chaffey G, Lloyd DJB, et al. Modelling and detecting tumour oxygenation levels. PLoS ONE. 2012; 7: 1–29.
8. Grimes DR, Fletcher AG, Partridge M. Oxygen consumption dynamics in steady-state tumour models. Royal Society open science. 2014; 1: 140080.
9. Daşu A, Toma-Daşu I, Karlsson M. Theoretical simulation of tumour oxygenation and results from acute and chronic hypoxia. Physics in medicine and biology. 2003; 48: 2829–42.
10. Mates vanLöbensels E, Anderson JC, Hildebrandt J, et al. Modeling diffusion limitation of gas exchange in lungs containing perfluorocarbon. Journal of applied physiology (Bethesda, Md : 1985). 1999; 86: 273–84.
11. Riess JG. Oxygen Carriers ("Blood Substitutes")Raison d'Etre, Chemistry, and Some Physiology. Chemical Reviews. 2001; 101: 2797–2920.
12. Vovenko E. Distribution of oxygen tension on the surface of arterioles, capillaries and venules of brain cortex and in tissue in normoxia: An experimental study on rats. Pflugers Archiv European Journal of Physiology. 1999; 437: 617–623.
13. Dewhirst MW, Ong ET, Rosner GL, et al. Arteriolar oxygenation in tumour and subcutaneous arterioles: effects of inspired air oxygen content. The British journal of cancer Supplement. 1996; 27: S241-6.
14. Torres Filho IP, Leunig M, Yuan F, et al. Noninvasive measurement of microvascular and interstitial oxygen profiles in a human tumor in SCID mice. Proceedings of the National Academy of Sciences of the United States of America. 1994; 91: 2081–5.
15. Waite CL, Roth CM. Nanoscale drug delivery systems for enhanced drug penetration into solid tumors: current progress and opportunities. Critical reviews in biomedical engineering. 2012; 40: 21–41.
16. Bae YH, Park K. Targeted drug delivery to tumors: myths, reality and possibility.

Journal of controlled release : official journal of the Controlled Release Society. 2011; 153: 198–205.
17. Wang M, Pan N. Predictions of effective physical properties of complex multiphase materials. Materials Science and Engineering R: Reports. 2008; 63: 1–30.
18. Zoabi N, Golani-Armon A, Zinger A, et al. The evolution of tumor-targeted drug delivery: From the EPR effect to nanoswimmers. Israel Journal of Chemistry. 2013; 53: 719–727.